Development of New Steels for Lightweight Construction

Clemens Neipp[1], Christian Weber[2], Holger Surm[3],
Wolfgang Bleck[1], Karsten Stahl[2],Thomas Tobie[2], Hans-Werner Zoch[3]

[1] Department of Ferrous Metallurgy, RWTH Aachen University, Intzestraße 1, 52072 Aachen
[2] Gear Research Centre, Technical University of Munich, Boltzmannstraße 15, 85748 Garching
[3] Stiftung Institut für Werkstofftechnik Bremen, Badgasteiner Straße 3, 28359 Bremen

1   Summary

This contribution deals with the influence of different carbonitriding parameters on the microstructure and mechanical properties of an enhanced case-hardening steel. The alloy is based on 18CrNiMo7-6, but microalloyed with vanadium and niobium. Gears, made from this carbonitriding steel, were thermochemically treated using different hardening and annealing temperatures, in addition to varying set points of carbon and nitrogen contents. The aim is to produce different types and amounts of precipitates and retained austenite in the case. Three variants, labeled A, B and C, were chosen from pretests and further analyzed using SOES, LOM, XRD, Vickers micro hardness tests, and tooth root bending tests. The microstructure shows finely dispersed retained austenite in a martensitic matrix, with the amount strongly dependent on nitrogen and carbon content. The precipitate state demonstrate a higher dependency on the annealing temperature than other process parameters. The hardness profile of variant A is similar to conventional carburized specimen, variants B and C show lower hardness values at the surface associated with high amounts of retained austenite. Nevertheless, variant B shows higher hardness and CHD than variants A and C. The tooth root bending strengths of all three variants show comparable results. Nevertheless, variant B shows a significantly lower result scatter than variants A and C.

Keywords

2   Introduction

The research project "Ultra High-Strength Lightweight Steels" concerns itself with the research, development and characterization of an improved case-hardening steel for gear applications. The goal, to enhance the power density of the material and thus support lightweight design, falls in line with the superordinate research network "Lightweight Forging".

At present carbonitriding is not a common thermo-chemical treatment to increase mechanical properties of gear. But in recent research projects promising results concerning the load-carrying capacity have been achieved [1-2]. Regarding tooth root bending strength, carbonitrided and carburized variants show similar values. But the investigations of carbonitrided variants result in increased pitting fatigue strength, especially at high retained austenite in the case.

For the heat treatment process of carbonitriding, the steel 18CrNiMo7-6 [3] was alloyed with niobium and vanadium. Together with the added carbon and nitrogen, carbides and nitrides are precipitated during heat treatment to improve the mechanical properties. Additionally, varying amounts of retained austenite in the case were produced, to prolong service life.

The effect of carbon and nitrogen content as well as the influence of hardening and annealing temperatures on the surface properties were analyzed by the means of factorial design of experiments. From a series of 17 heat treatment procedures, three variants, furthermore labeled as variants A, B and C, were chosen for mechanical pretests. The selection criteria for the variants were the amount of retained austenite and precipitates in the surface area. Later on, the best performing of these three variants is chosen for further analysis and will be compared to industrial standards.

3   Methods and Material

The chemical composition was derived from 18CrNiMo7-6, as specified in [3], with the addition of niobium and vanadium. Niobium precipitates are stable up to high temperatures and can effectively hinder the grain coarsening during carbonitriding. The vanadiumcarbonitrides are precipitated in the temperature range of hardening, which allows to easily influence the precipitate distribution. The aluminum and sulfur contents were set specifically low to achieve high metallographic cleanliness and thus promote a long service life. Other element contents were set as the mean value of the respective element´s tolerance in [3]. The tolerances and the actual chemical composition of the case-hardening steel ingot are given in Table 1.

Steel grade	C	Si	Mn	Al	Cr	Mo	Ni	V	Nb	B
18CrNiMo7-6	0.15 0.21	max 0.40	0.50 0.90	-	1.50 1.80	0.25 0.35	1.40 1.70	-	-	-
CN-Steel	0.19	0.31	0.70	0.025	1.65	0.31	1.55	0.10	0.03	0.003

Table 1:   Nominal composition of steel grade 18CrNiMo7-6 according to [3], and actual chemical composition of the investigated carbonitriding steel, denoted as CN-Steel (in percentage by weight)

An 80 kg ingot was vacuum induction melted and cast into a permanent copper mold with a base of 140x140 mm^2. Austenitization of the ingot was performed at 1250 °C for 120 min, then forged to an 80x80 mm^2 base and air-cooled to room temperature.

From the forged ingots small specimen were cut to the dimensions 15x15x10 mm^3 for SOES and XRD analysis, as well as test gears for mechanical testing. The main nominal test gear geometry is given in Table 2.

Denomination	Symbol	Unit	Value
Module	m_n	mm	2.0
Face width	b	mm	10
Number of teeth	z	-	29
Pressure angle	α_n	°	20
Helix angle	ß	°	0
Tip diameter	d_a	mm	64.7

Table 2:   Main nominal test gear geometry

The schematic time-temperature sequences for carbonitriding are shown in Figure 1. The specimen and test gears were preheated to 850 °C, carbonitrided at 940 °C and hardened at 850 °C or 800 °C (T_H). During carbonitriding the carbon potential C_p and ammonia flow rate were regulated to ensure a carbon content of 0.8 wt% or 0.6 wt%, and a nitrogen content of 0.5 wt% or 0.3 wt% at a depth of 100 µm below the specimen surface. The hardening temperatures were chosen to produce favorable distributions of vanadium precipitates in the microstructure. After oil-quenching the specimen and test gears were annealed at 150 °C or 210 °C (T_A) and air-cooled to room temperature. The tooth root area of all test gears was shot peened with rounded cut wire after heat treatment.
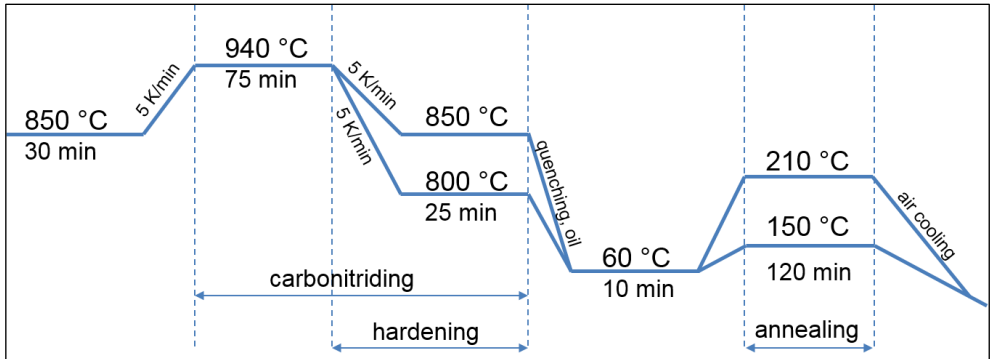

Figure 1:   Time-temperature profiles utilized in carbonitriding of the specimen and test gears

Carbon and nitrogen profiles were evaluated via spark optical emission spectroscopy (SOES) using an ARL[TM] 3460 optical emission spectrometer.

The phase fraction of martensite, retained austenite, carbides, and nitrides were determined with x-ray diffraction in a distance of 100 µm from the surface. The measurement was done with a diffractometer Siemens type D500 using Cu-Kα radiation with primary aperture of 1.0° / 0.3°. A 2θ-range from 20° to 120° was scanned using an increment of 0.03°, and a step time of 50 s. Counts were recorded with a scintillation counter. The analysis of the diffraction patterns was done with Rietveld software Topas 4.2, Bruker-AXS.

Vickers micro hardness (HV1) was used to measure CHD_{550} and hardness profiles.

The tooth root bending strength of the test gears was determined by bending fatigue tests. The test gears were clamped symmetrically and tested over five teeth between two jaws. Flank angle deviations were compensated by the means of a precision adjustment, so that a uniform load distribution across the whole face width could be assumed.

According to [4], the nominal tangential load, F_t, is determined in the transverse plane at the reference cylinder, and is derived from the nominal torque transmitted by the gears. In case of gears with normal addendum geometry, following [4], the maximum tooth root stress is assumed when load is applied at the most external point of the single pair tooth contact. For calculating the nominal tooth root stress σ_{F0} in a pulsating load test, the adapted equation according to [5] is used. Thereby the tangential force F_t is replaced by the pulsating load F_{Pn}, applied normal to the flank surface. For each variant between 8 and 9 tests were performed in the region of endurance life following the stairstep-method described in [6].

3

4 Results

The characteristics of the three variants chosen for the first mechanical tests are listed in Table 3. Variant A has the lowest amount of retained austenite, variant B the lowest phase fraction of precipitates and a medium amount of retained austenite. In variant C, the highest amounts of both retained austenite and precipitates were measured.

measurement	variant A	variant B	variant C
Carbon [wt%]	0.61	0.73	0.81
Nitrogen [wt%]	0.35	0.30	0.50
T_H [°C]	850	850	800
T_A [°C]	210	150	210
Precipitates [vol%]	8.2	7.9	11.4
γ_R [vol%]	15	24.3	30.7

Table 3: Measured carbon and nitrogen content, set hardening (T_H) and annealing (T_A) temperatures during heat treatment, and measured precipitate and retained austenite (γ_R) phase fractions, taken at 100 µm distance from the surface

The carbon and nitrogen profiles in the case-hardened layer of the three variants are documented in Figure 2. In all variants, the carbon and nitrogen profiles show similar characteristics. The carbon profiles are indicated by a small plateau at the surface and a continuously decreasing carbon content towards the core. Except for variant B, all carbon content set points are reached. The nitrogen distribution is characterized by a large concentration gradient in the first 200 µm. Nevertheless, the actual nitrogen contents at a distance of 100 µm from the surface are close to the set points.
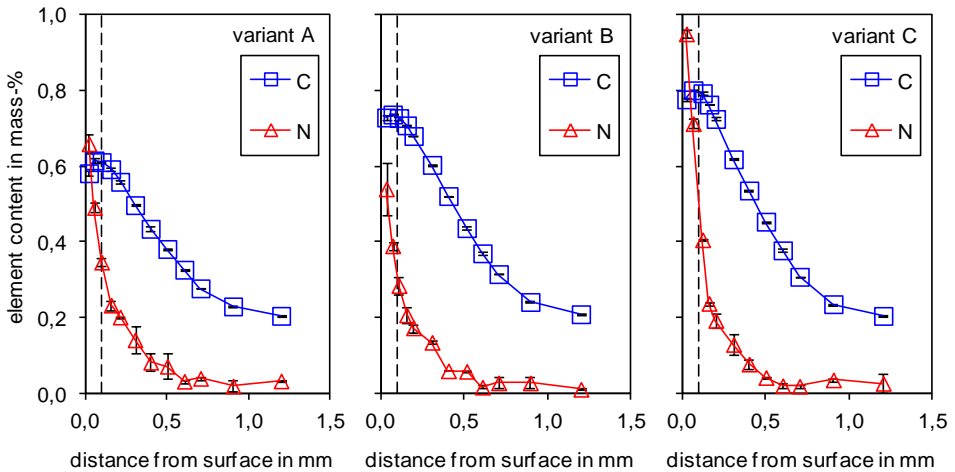

Figure 2: Carbon and nitrogen distribution in the case-hardened layer of the three variants, broken line indicates 100 µm distance from the surface

The microstructure after carbonitriding is particularly influenced by the amount of retained austenite (Figure 3). The phase fraction of retained austenite in the carbonitrided layer increases in the order of variant A to variant C. The retained austenite is finely dispersed in the martensitic matrix. But the identification of the desired

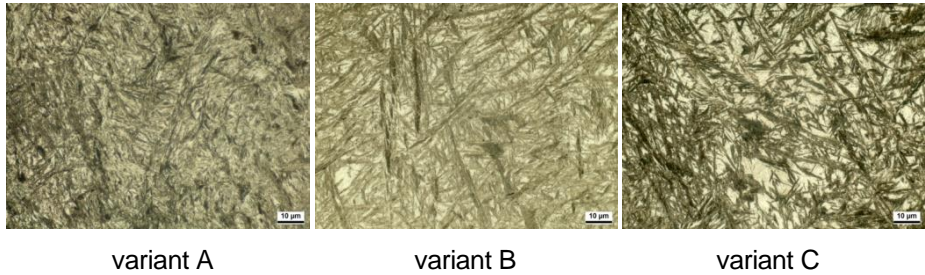precipitations was not possible with OLM and had to be realized by XRD measurements.

<div align="center">variant A   variant B   variant C</div>

Figure 3: Microstructure of the carbonitrided steel after heat treatment (etching: 35 s, 3% alk. HNO_3; sampling: longitudinal), taken at 100 µm distance from the surface

The results of XRD analysis are shown in Figure 4 and Figure 5. Figure 4 summarizes the different phase fractions of martensite, retained austenite, nitrides and carbides. It can be seen, that the different processes affect the amounts of martensite and retained austenite the most, while the amount of nitrides and carbides varies by only 3 %.
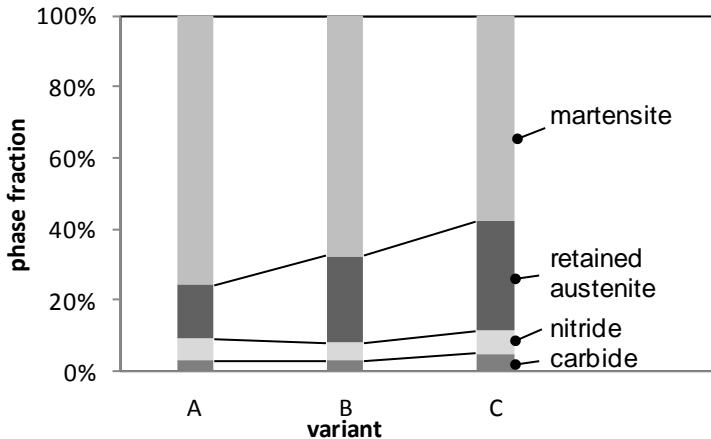

Figure 4: Phase fraction of martensite, retained austenite, nitrides, and carbides, measured at 100 µm distance from the surface

The amount and types of precipitated carbides and nitrides, depicted in Figure 5, differ vastly between the three variants. Especially the amounts of the nitrides CrN and $Fe_{16}N_2$, as well as of the carbides VC and Fe_3C seem very susceptible to the utilized process parameters.
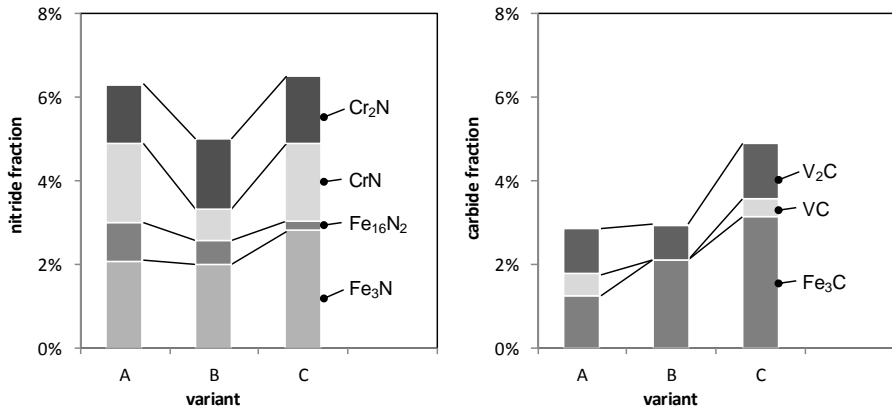
Figure 5: Phase fraction of different nitrides and carbides, measured at 100 μm distance from the surface

The process parameter variation also results in different hardness patterns, depicted in Figure 6. The hardness profile of variant A is very similar to common carburizing processes, characterized by a surface hardness of 700 HV1 and a continuous decrease. Variants B and C show an increasing hardness at first, caused by high retained austenite fractions, followed by the same decrease as variant A. In addition, the maximum hardness of these two variants differ from 760 HV1 in variant B to 680 HV1 in variant C. Variant B also has the highest CHD_{550} of 0.74 mm, whereas variants A and C are close to each other with a CHD_{550} of 0.61 mm and 0.63 mm, respectively.
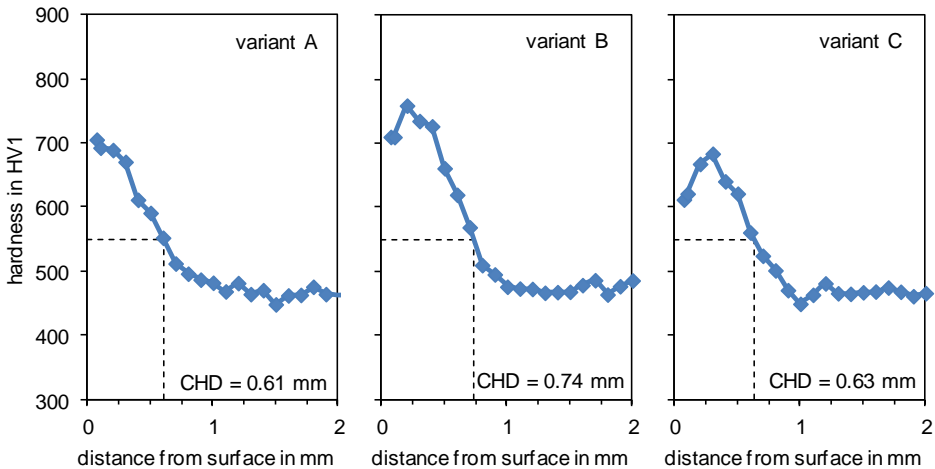

Figure 6: Hardness profile and CHD_{550} in the case-hardened layer of the three variants

The test results for tooth root bending strength are shown in Figure 7. All three investigated variants show a comparable tooth root bending strength that surpasses the defined quality range according to ISO 6336 [4]. This is in good accordance to the experience for shot peened gears of this design size. Nevertheless, only on variant B no tooth root breakages occur at a nominal tooth root stress σ_{F0} = 1590 N/mm² so far.

6

Attention should also be paid to the different scattering which is significantly lower for test variant B than for variants A and C.
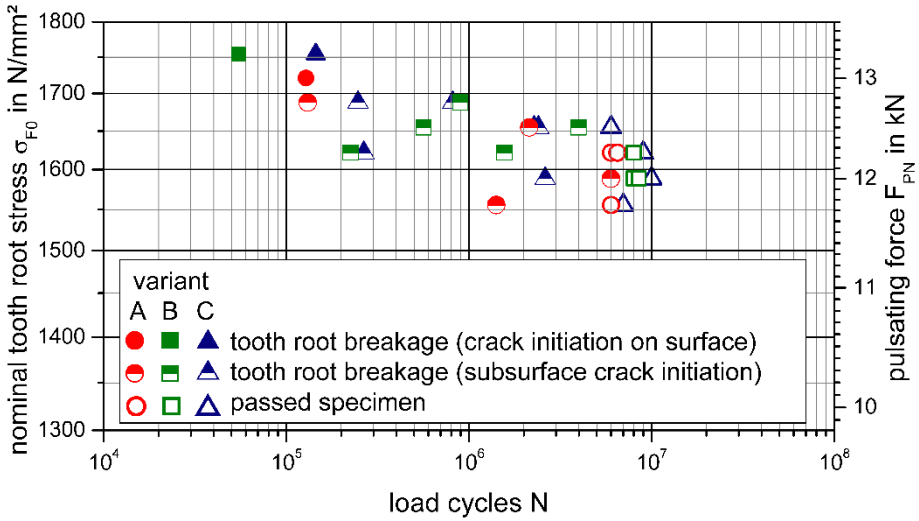

Figure 7: Tooth root bending test results for Variants A, B and C

5   Discussion

Different phase fractions of martensite, retained austenite, carbides and nitrides in the surface were achieved by controlled variation of the heat treatment parameters. Also, high carbon and nitrogen contents support a higher amount of retained austenite and a lower proportion of martensite, respectively. The amount and types of precipitated nitrides and carbides strongly depend on the contents of nitrogen and carbon, but also hardening and annealing temperature. The highest fraction of iron nitride, Fe_3N, is measured if high nitrogen contents are realized. The precipitation of cementite, Fe_3C, shows the same behavior regarding carbon content. Although the total number of heat treatment variants is too small to identify clear effects on the precipitation behavior, the sum of nitride precipitations seem to be strongly influenced by the annealing temperature. The fraction of chromium nitride, CrN, is the lowest in variant B, which was annealed at 150 °C. Additionally, no vanadium carbide, VC, is found in this variant. The effect of retained austenite on the micro hardness is seen in Figure 6. The initially low hardness of variant B and C is caused by the high amount of the comparatively soft austenite, which decreases with rising distance from the surface. The increasing amounts of martensite then cause higher measured hardness.

In case of fatigue tests a fracture surface can be divided between a fatigue zone and a fast fracture zone. Since the crack grows in a transcrystalline way after initiating, the fatigue fracture area is smooth. After the crack reaches a sufficient length an overload breakage happens, then crack grows in an intercrystalline way, thus the residual crack surface looks ragged. For all test runs, most of the cracks were initiated from underneath the component surface. This is in good accordance with the test results of current research work which show subsurface cracks on shot peened heavy-duty gears [7-9]. To determine the reasons for this subsurface cracks, further metallographic investigations on the test gears have to be done.

6   Conclusions

The combination of the microalloying elements and the adapted carbonitriding heat treatment allowed us to produce very different precipitation states and varying amounts of retained austenite in the surface area of the carbonitriding steel. Hardness profiles and CHD_{550} show favorable mechanical properties for gear applications. For a further evaluation of the bending fatigue test results analysis of the fracture surfaces, to identify the crack initiation cause, as well as XRD analysis in the shot peened tooth root area are necessary and intended.

References:

[1] Steinbacher, M., Hoffmann, F., Lombardo, S. and Tobie, T.: HTM J. Heat Treatm. Mat. 70 (2015) 5

[2] Lombardo, S., Tobie, T., Stahl, K., Steinbacher, M. and Hoffmann, F.: HTM J. Heat Treatm. Mat. 70 (2015) 5

[3] DIN EN 10084: Case hardening steels – Technical delivery conditions, 2008

[4] ISO 6336: Calculation of load capacity of spur and helical gears, part 1-5, 2006/2016

[5] FVA-Richtlinie: Vereinheitlichung von Tragfähigkeitsversuchen (FVA 563 I), 2012

[6] Hück, M.; Bär, S.; Schütz, W.: Verbesserung der statistischen Aussagefähigkeit von Dauerfestigkeitsversuchen (Treppenstufenverfahren), IABG-Bericht Nr. TF-651 B, 1977

[7] Bretl, N.: Einflüsse auf die Zahnfußtragfähigkeit einsatzgehärteter Zahnräder im Bereich hoher Lastspielzahlen, Dissertation Technical University of Munich, 2010

[8] Bretl, N., Schurer, S. Tobie, T. Stahl, K. and Höhn, B.-R.: Investigations on Tooth Root Bending Strength of Case Hardened Gears in the Range of High Cycle Fatigue, AGMA Technical Paper, 2013

[9] Schurer, S.: Einfluss nichtmetallischer Einschlüsse in hochreinen Werkstoffen auf die Zahnfußtragfähigkeit, Dissertation Technical University of Munich, 2016

Lightweight gearwheel design using separate gear ring and wheel body
Part I: Joining by heat treatment and testing

Authors:
C. Leonhardt[1], M. Otto[1]; K. Stahl[1], D. Nadolski[2], H. Surm[2], M. Steinbacher[2] and H.-W. Zoch[2]

[1] *Institute of Machine Elements (FZG), Technical University of Munich, Germany*
[2] *Foundation Institute of Materials Science (IWT), Bremen, Germany*

Abstract

Due to increasing stringent restrictions concerning the exhaust emissions until the year 2020 the automobile manufacturers aim to reduce the CO_2-emissions. In the past, the focus of weight reduction efforts was set on the car body and resulted in very case-specific solutions. Recent investigations show high potential for weight reduction of the powertrain. A very promising weight reduction concept is the intelligent lightweight design through multi-component processes. In actual terms this approach replaces the conventional gear concept by a high-strength gear ring and a wheel body using lightweight design structure. The teeth on the gear ring have to withstand high local loads in the tooth contact.

The necessary interference fit has to be calculated with respect to the transferred torque value and the strength of the gear ring, especially tooth root strength. A central process of the multi-component gear design is the joining process of the single components that can be realized by a friction type press fit supported by the heat of the previous case hardening process. An important point is the effect of case-hardened depth on size change of the gear ring. The joined gears will be checked on a static torque test device in order to determine typically occurring failure modes and to pick promising variants with best gear performance.

1   Introduction

The weight of powertrain components has been continuously reduced by load-adapted design and through material savings achieved in regions with low stress. With the consistent increase in power density and associated reduction in weight, additional potential is available for the intelligent lightweight design of powertrain components in future. Significant potential is offered by taking an integrated look at part design, material, heat treatment as well as the production and joining processes used. By combining various production processes and materials, the different requirements placed on various component areas are fulfilled in a targeted way. This enables lightweight design which is adapted to the acting load and is cost-efficient.

High power density and low part weight are achieved with gears designed with the use of high-strength steel for a gear ring in combination with a low weight wheel body.

The wheel body can be produced from ultra-high-strength sheet materials with very low weight. Through deep drawing, very light wheel bodies with thin wall thicknesses are attained. Furthermore, stacking of blanked sheet parts yields a weight saving due to a load-optimized wheel body structure. The advantage of such a design (differential design) compared to an integral one lies in the ability to combine optimized processes for generating individual components with a load-adapted design. The differential design approach is demanded on lightweight

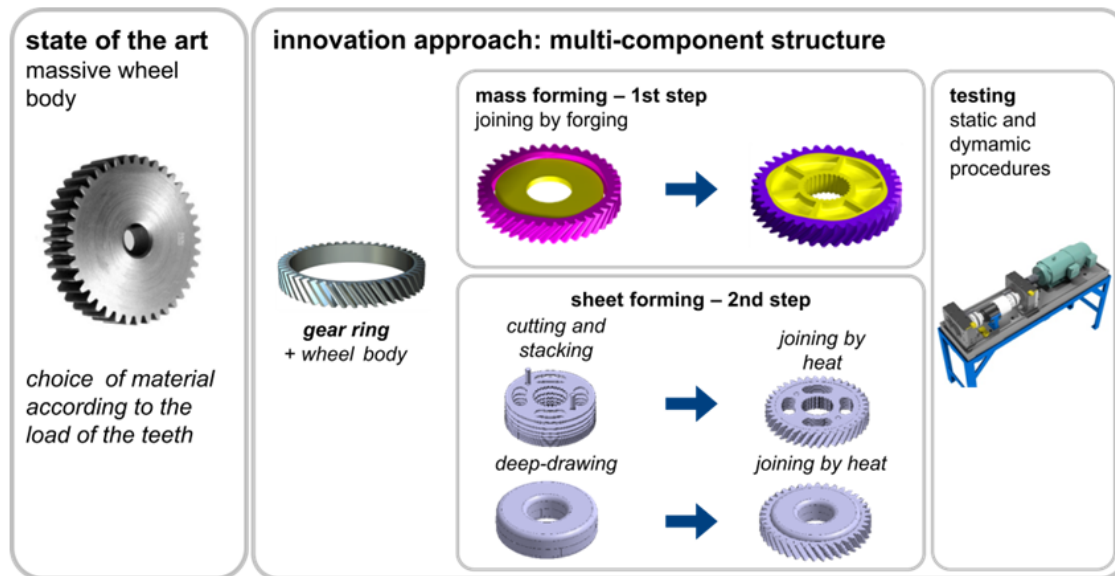gearbox applications for transportation systems and aerospace or in noise-critical applications [1], [2].

Figure 1.1: Design approach for multi-component gears

One of the main challenges is the joining of the gear ring with the wheel body. In this project different joining strategies are investigated to achieve multi-component gears with the highest possible mechanical properties.

One of the strategies is the integration of the joining process into the heat treatment process. The thermal joining of a press fit between the case-hardened gear ring and wheel body can be achieved efficiently through specifically exploiting temperature differences directly during the quenching process. Since the treatment process usually causes also undesirable distortion [4], [5] this size and shape changes must also be taken into account for the joining process. Another investigated strategy is the joining by lateral extrusion which will be shown in the second part.

2   Multi-component gear design

The gearwheel in these investigations consists of the wheel body, which is the focus in the second part, and the gear ring. The geometry of the gearing (module: 2 mm, helix angle: 30°) is based on common automotive applications, only the center distance between the meshing gears is adapted to the requirements of the test rigs used. The material of the gear ring is a high strength case-hardened steel (18CrNiMo7-6).

2.1   Joining by Heat Treatment

A central process of the multi-component gear design is the joining of the single components by a friction type press fit supported by the heat of the previous case hardening. The connection between the gear ring and the wheel body is realized exactly during the quenching process of the gear ring. For this operation a special heat treatment set-up and procedure is necessary. In a first step the gear rings are carburized to the desired surface carbon content of approximately 0.7 mass-% at temperatures between 900 and 940 °C. After the temperature decrease to the hardening temperature of 850 °C the gear rings are withdrawn from the furnace and transferred to a gas nozzle-field where the parts are gas quenched with

nitrogen (4000 l_n/min) for 60 s. The heat treatment procedure is shown in **Fehler! Verweisquelle konnte nicht gefunden werden.**.1.

The first part of the investigations deals with the fundamental distortion behavior of the gear ring without consideration of the wheel body. For this the influence of the case hardening depth (CHD = 0.3; 0.5; 0.7; 0.9 mm) on the outside (measured on the tip of tooth) and inside radius changes of gear rings was analyzed. Geometrical measurements were conducted on a coordinate measuring machine before and after the heat treatment. After the determination of the size changes the dimensions before the heat treatment were readjusted by taking into account the necessary press fit.
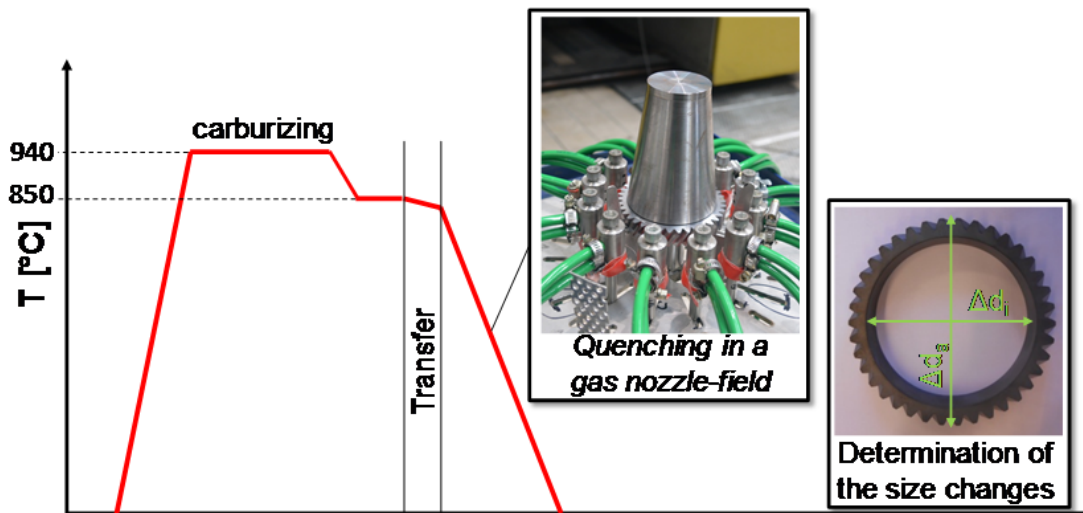

Figure 2.1: Schematic representation of the process chain "joining during quenching"

The first joining tests were carried out with machined solid wheel bodies from the same material as the gear ring (18CrNiMo7-6). This wheel body variant has no lightweight potential and should only show the performance of the joining. In the future, this solid wheel body can then be exchanged by other lightweight concepts (figure 1.1). For the joining operation the wheel body is placed in the centre of the gas nozzle-field in the same height where later the hot gear ring is placed. A mounted conical feed over the wheel body guarantees a centric positioning of both parts. Due to thermal expansion of the gear ring at 850 °C there is a joint play of over 700 µm between gear ring and wheel body before the gas quenching starts. Furthermore the joint play can be additionally increased by a prior cooling of the wheel body. So the first experiments were carried out with wheel bodies, which were placed at room temperature in the centre of the gas nozzle-field. In a second variant, the wheel body was cooled down in liquid nitrogen to -196 °C prior to the joining process.

2.2 Testing procedures of multi-component gears

A lightweight gear design can only be advantageous if it provides the same transmittable power or comes up with other convenient characteristics such as a superior dynamic behavior. In order to prove assembled gears to be a promising concept, prototype tests have to be conducted. Therefore different test methods have been developed to determine the characteristics of multi-component gears in comparison to a conventional massive gear and to find out their limits. In the context of the research project "Lightweight Forging Initiative" [8] various variants will be manufactured and tested to find the best concept.

2.2.1 Static load capacity

The first test is a static test to determine the maximum torque that can be sustained by the multi-component gear. Therefore, the gear is mounted on a shaft meshing with a second massive gear that is designed to be stronger in order to withstand the load (figure 2.2). During the test procedure the multi-component gear is loaded with continuously increasing torque, which is produced by a motor driven lever mechanism. To detect the failure behavior of the test gear measuring equipment is applied to the test rig.

A torque measuring shaft directly mounted to the shaft of the test gear records the torque load that is introduced and likewise a major failure criterion of this test. On the other side of the gear shaft a rotary encoder captures the kinematics of the shaft and therefore the torsional deformation of the gearwheels. By comparing the measurement results for different arrangements, the deformation of the test gears can be derived.
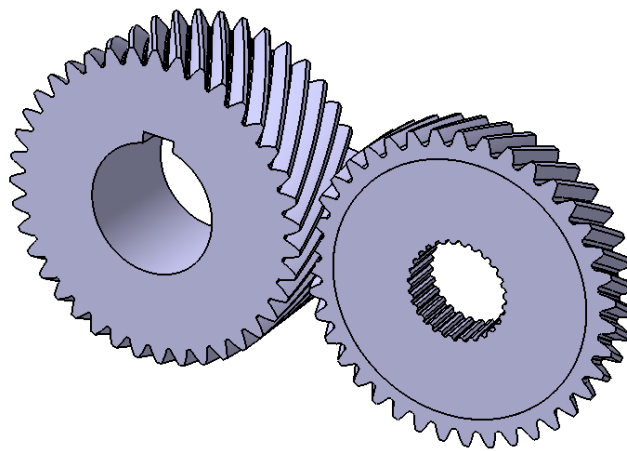

Figure 2.2: Testing configuration of the static load capacity test

The increasing load on the test gear may lead to different failure scenarios. The press fit between the wheel body and the gear ring limits the transmittable torque that is defined by the coefficient of friction and the compressive stress in the joint. Once the maximum torque is exceeded the gear ring starts to slip on the wheel body, which is no structural failure but a loss of functionality. Since the teeth of the test gears are designed with a helix angle typically for automotive application the axial force in the contact can affect the gear ring to be pushed axially off the wheel body. Another failure mode is the tooth root breakage [3]. The tooth root stress of a multi-component gear with press fit directly under the teeth is composed of two stress components. The static part of the stress is a tangential stress component that is induced by the compressive stress in the press fit of gear ring and wheel body. The second component is the tooth root bending stress due to the tooth normal force. If the superposition of these stress components exceeds the material strength and the friction forces in the joint are large enough to prevent the gear ring from slipping, the tooth root can break. Another failure mode that can occur especially on the form-fit wheels is the breakage of the gear ring.

The recording of the torque and the rotary angle of the test gear shaft on the same time base enables the detection of the torque at which a potential failure occurs. Since the conduction of this test takes only short time it is suitable to test a large number of test gears. Therefore the test is meant to be a screening test to extract the gears with the highest load capacity. The most promising specimens will get

into further testing with the following test methods to determine their overall characteristics.

2.2.2   Dynamic characteristics and lifetime behavior

Besides the static load carrying capacity the dynamic behavior and the durability are an important issue in application of gears. Therefore running tests on a modified FZG-back-to-back test rig with a center distance of 91.5 mm are conducted. In these tests selected specimens that showed best results in the static test procedure are examined. This test reproduces the conditions of a subsequent application best hence the load acts circumferential around the gear. Potential failure modes besides the slip in the joint and a tooth root breakage can be the typical damages on the flank (e.g. pitting or micropitting). Due to the moving load and subsequently deformation of the gear ring the slipping torque is expected to be lower compared to the results in the static case.

The noise behavior of the multi-component gear design is captured with acceleration sensors applied to the housing near the bearings in contact direction. The recording of the acceleration signal allows the relative assessment of the different wheel body designs in terms of damping and noise emission.

2.2.3   Static deformation tests

The third test procedure is also based on a static loading of the gear. But in contrast to the first two test methods it aims not to produce failure on the gear and therefore is nondestructive. As the weight optimized wheel body shows a reduced stiffness in contrast to its massive counterpart, the deformation of the multi-component gear is the focus of the static deformation test. These tests are conducted on a coordinate measuring machine. The load-induced deviation of the flank position can influence the contact pattern of the meshing gears. Consequently the results can be used to estimate the load on the flank and subsequently design an appropriate profile modification [6].

3   Results and Discussion

3.1   Joining by heat treatment

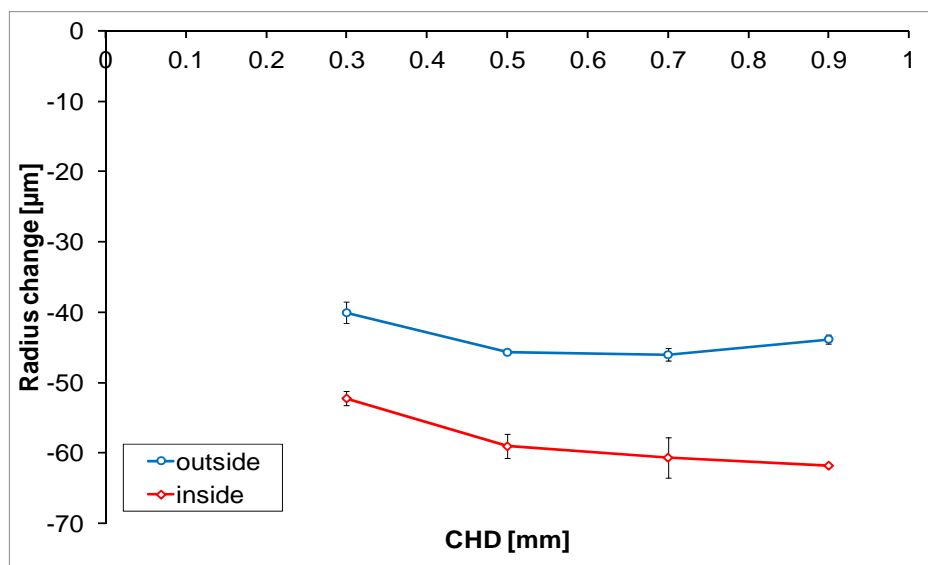#### 3.1.1   Influence of the CHD on the dimensional changes

Figure 3.1: Influence of the CHD on the outside and inside radius change of the gear rings

The preliminary investigations were carried out on the gear ring without a wheel body. Figure 3.1 shows the influence of the case hardening depth on the size changes of the gear ring. The heat treatment reduces both, the inside and the outside radius.

The knowledge of inside radius changes is essential for the further joining operations but also the outside radius changes are important because in further investigations only this dimension can be measured on a joint gear. Since a small effect of the case hardening depth on the size changes is visible for the joining operation only the CHD = 0.5 mm was chosen.

3.1.2 Joining of the gear ring and machined wheel body

After the dimensional changes of the gear ring have been determined the outer diameter of wheel body was readjusted to meet the required press fit of 100 μm between gear ring and wheel body at room temperature.
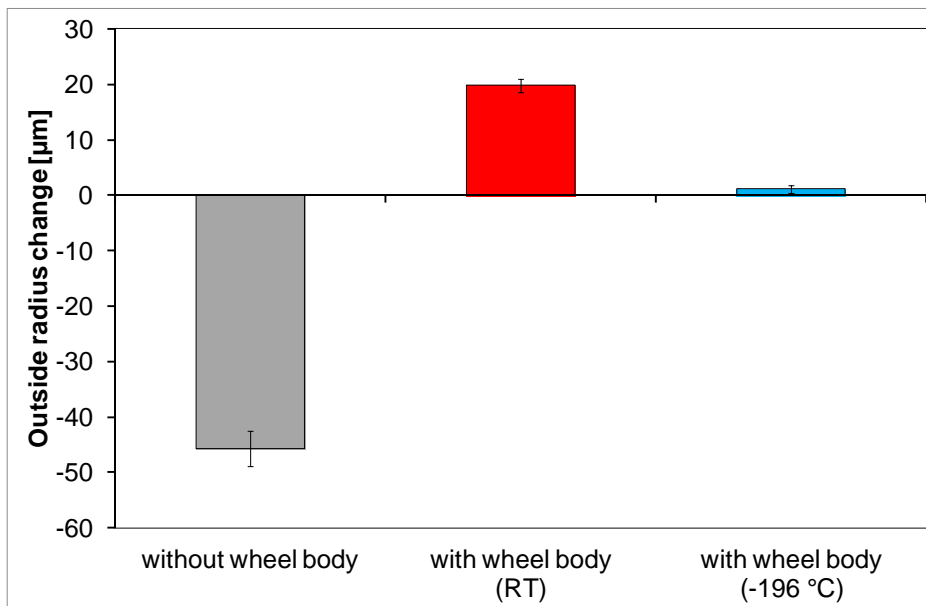

Figure 3.2: Outside diameter changes of the freely quenched and joint gear ring (CHD 0.5 mm)

In figure 3.2 the outside radius change for a freely quenched gear ring is juxtaposed with size changes of joint gears. While a freely quenched gear ring exhibits a radius reduction of -46 μm for the joint variant radius increases of over +20 μm occur. It must be taken into account that plastic deformations can occur during the quenching process when the hot gear ring comes into contact with the wheel body. A prior cooling of the wheel body leads to a different size change behavior; after the heat treatment nearly no radius changes appear. By reducing the temperature of the wheel body the diameter can be temporarily decreased and therefore the moment when the gear ring gets contact to the wheel body can be delayed. Since during the first contact the gear ring is at a lower temperature premature plastic deformation can be avoided. In contrast to the not cooled variant nearly no outside radius changes occur.

Due to the small wall thickness of the gear ring not only average diameter changes but also roundness deviations can occur. Fourier analyses were carried out to determine amplitudes of corresponding trigonometric functions of different Fourier orders [7]. Figure 3.3 shows the distortion behavior of the outer diameter for the three variants.

In spite of uniform quenching conditions an average roundness change of nearly 40 µm amplitude in the second Fourier order (ovality) is identified for the freely quenched variant. Small amplitudes are also identified for the Fourier orders 3 (triangularity) und 4 (rectangularity). By quenching the gear ring on the wheel body roundness deviations can be significantly reduced. The improvement of the dimensional accuracy is regardless of the wheel body temperature.
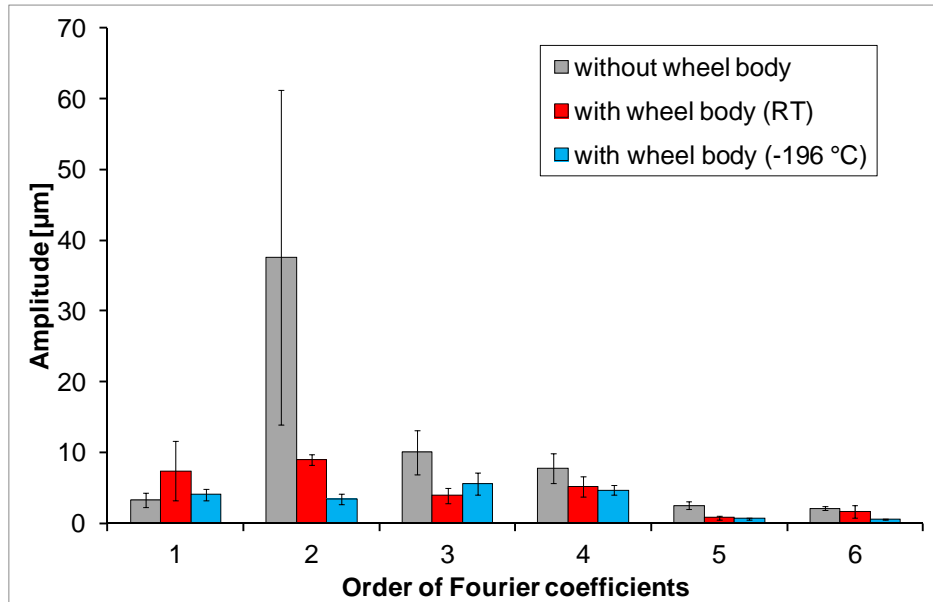

Figure 3.3: Distortion of the outer diameter; Fourier spectra

4   Summary

First experiments showed that joining of a high strengths gear ring on a wheel body during the quenching process is possible (figure 4.1). However, it must be considered that during the contact with the wheel body plastic deformations in the hot gear ring can occur. On the one hand these plastic deformations may be considered positive since they reduce the roundness deviations. On the other hand they can contribute to an additional expansion of the inside diameter and thus to a reduction of the press fit. For this reason, the conduction of different tests is planned for the multi-component gears. The test methods contain static and dynamic load as well as destructive and nondestructive test. The different focus of these tests enables a very comprehensive investigation of the properties of this innovative design approach. In further investigations the solid wheel body will be substituted by different lightweight concepts that will be shown in a second paper.

Figure 4.1: During heat treatment joint gear and tasks for further investigations

5 Acknowledgements

6 References

[1] Aziz, I.A.A., Idris, D.M.N.D., Ghazali, W.M.: Investigating bending strength of spur gear: A review, (2016) MATEC Web of Conferences, 90, art. no. 01037.

[2] Brecher, C., Gorgels, C., Hesse, J.: Light and silent: Noise reduction using material compound gears, (2008) VDI Berichte, (2029), pp. 627-645.

[3] Schinagl, S.: Zahnfußtragfähigkeit schrägverzahnter Stirnräder unter Berücksichtigung der Lastverteilung, Dissertation, TU München, 2002

[4] Steinbacher, M.; Surm, H. Clausen, B.; Lübben, Th., Hoffmann, F.: Systematische Untersuchung verschiedener Einflussgrößen auf die Maß- und Formänderungen von einsatzgehärteten Stirnrädern, Teil 1: Grundkörperverzug. HTM J. Heat Treatm. Mat. 67(2012)1.

[5] Steinbacher, M.; Surm, H.; Clausen, B.; Lübben, Th.; Hoffmann, F.: Systematische Untersuchung verschiedener Einflussgrößen auf die Maß- und Formänderungen von einsatzgehärteten Stirnrädern - Teil 2: Verzahnungsverzug. HTM J. Heat Treatm. Mat. 67(2012)4

[6] Neubauer, B.; Weinberger, U.: FVA-Nr. 571/II-Heft 1197 – Berechnung der Lastverteilung in Getriebesystemen mit beliebig angeordneten Planetenstufen. Forschungsvereinigung Antriebstechnik e.V., Frankfurt/Main (2016)

[7] Surm, H.; Frerichs, F.; Hoffmann, F.; Zoch, H.-W.: Erweiterte Verzugsanalyse am Beispiel von Wälzlagerringen; HTM J. Heat Treatm. Mat. 63(2008)2

[8] www.massiverleichtbau.de/en/startseite. (2017, February 10)

Lightweight gearwheel design using separate gear ring and wheel body
Part II: Different manufacturing concepts for replacing a full body gearwheel

Authors:
R. Meissner[1a], M. Liewald[1], T. Benkert[2] and W. Volk[2]

[1] Institute for Metal Forming Technology, University of Stuttgart, Germany
[2] Institute of Metal Forming and Casting, Technical University of Munich, Germany

Abstract

This paper presents two wheel body concepts for multi-component gearwheels, consisting of a gear ring and the already mentioned wheel body. Two process chains for manufacturing two wheel bodies are introduced. Additionally, both wheel bodies are investigated numerically. The torque between shaft and gearwheel a multi-component gearwheel is able to transfer is chosen as command variable to be maximized. Finally, both wheel body concepts are compared to each other.

1   Introduction

Funded by the Federal Ministry of Economic Affairs and Energy (BMWi) via the German Industrial Federation of Industrial Research Associations (AiF), the joint research project "Lightweight Forging" started in May 2015. In the context of this project, lightweight potentials of forged components are investigated in five work packages using different methods. In order to identify and to make use of lightweight potential of forged parts, networking of several stages of production becomes essential. The work package „Intelligent lightweight design through multi-component processes", run by the Gear Research Centre (FZG) of the Technical University of Munich, investigates the potential of using assembled gearwheels. A common gearwheel is divided into three parts – gear ring, wheel body, and shaft – so in this paper the substitution of the wheel body will be investigated using three different manufacturing processes. In these investigations, special heat-treated gear rings provided by the Institute of Material Science (IWT, Bremen) are used. The Institute of Metal Forming and Casting (utg, Munich) of the Technical University of Munich deals with a wheel body made of stapled sheet metal and one made by deep-drawing. These two wheel bodies are joined with the gear ring at IWT using the gear ring's shrinking after heat treatment. The Institute for Metal Forming Technology (IFU, Stuttgart) of the University of Stuttgart deals with wheel bodies manufactured by lateral extrusion (forging). Wheel body and gear ring are joined directly by one single forging stroke.

This paper focuses on the joining process and achieved properties for forged and stapled sheet metal wheel bodies. Manufacturing processes and numerical models to predict their load potential are introduced here. Furthermore, both wheel bodies are compared to each other.

2   Process routes for multi-component gearwheels

This chapter describes two processes to produce multi-component gearwheels. Gear ring and shaft provide geometrical boundaries for the different wheel bodies. The gear ring is 14 mm wide and has a maximum inner diameter of 77 mm. For forged wheel bodies the gear ring's inner diameter is of complex shape. Stapled sheet metal wheel bodies use gear rings with the above values and cylindrical in-

ner geometry. Both wheel bodies fit onto a DIN 5480-WAx30x1x28xh6x9e gear shaft

2.1 Stapled sheet metal wheel body

Figure 2.1 shows the process chain to manufacture a gearwheel with a stapled sheet metal wheel body. First, the wheel body's inner geometries are laser cut out of a large blank that is cut into smaller pieces in the same step. Inner geometries are the gear shaft geometry, four holes for aligning pins and specially designed holes to reduce the wheel body's weight. Since the sheet metal's outer circular geometry becomes a functional surface for the press fit between gear ring and wheel body, it is made by fine blanking. This special cutting technique allows generating nearly rectangular sheared edges with close to 100 % clean-shear share and very low surface roughness. One single sheet metal layer is 1.5 mm thick. Therefore, to achieve the wheel body's width, nine sheet metal layers are stapled. To join the wheel body and gear ring at IWT the wheel body's sheet metal layers have to be aligned and fixed. This is done by driving alignment pins through two of the laser cut round holes and two connectors through the other two holes. After tightening the connectors, retracting the alignment pins allows applying another two connectors to the wheel body. At IWT the two parts are joined directly after the gear rings heat treatment. With decreasing temperature, the gear ring shrinks onto the wheel body.
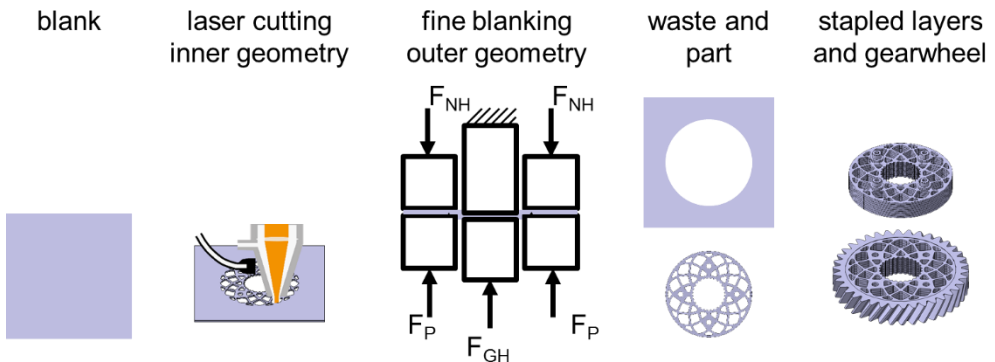

Figure 2.1: Process chain to manufacture gearwheel with stapled sheet metal wheel body

2.2 Lateral extruded (forged) wheel body

The forging process of an assembled gearwheel will be performed by laterally extruding a blank, placed between shaft and gear ring. Therefore, both the wheel body and the gear ring have to be prepared separately. Corresponding process route is shown in figure 2.2. First, the blank preparation starts with cutting slices of 9 mm height followed by piercing. Outer diameter and inner diameter have been chosen to be 72.0 mm and 27.8 mm while both do not have to be prepared with exact tolerances. Prior forming process, a conventional lubricant needs to be applied.

For the forming process, a completely finished gear ring is used. The gear hobbing and the hardening have to be therefore conducted before joining. Additionally, an out-of-round turning process is added in order to obtain an epitrochoid profile on in the inner side of the gear ring. This profile is combined with an extra cavity to enable a form and force fit in tangential and axial direction. Since this kind of undercut and non-circular shape cannot be manufactured on conventional turning or milling

machine, the test pieces were provided by J.G. Weisser Söhne GmbH & Co. KG in St. Georgen (Germany).

The actual joining process is performed with a one-stage hydraulic press. The gear ring is placed between six preloading die segments preventing impermissible tangential tension stress of the gear ring while and after forming. The blank is placed between two punches and is guided by the inner mandrel. The lateral extrusion process is initiated and conducted by the upper punch. In order to obtain a symmetric homogenized lateral extrusion process on a one-stage hydraulic press a hydraulic closing device, equipped with hydraulic chamber and nitrogen storages, is used.
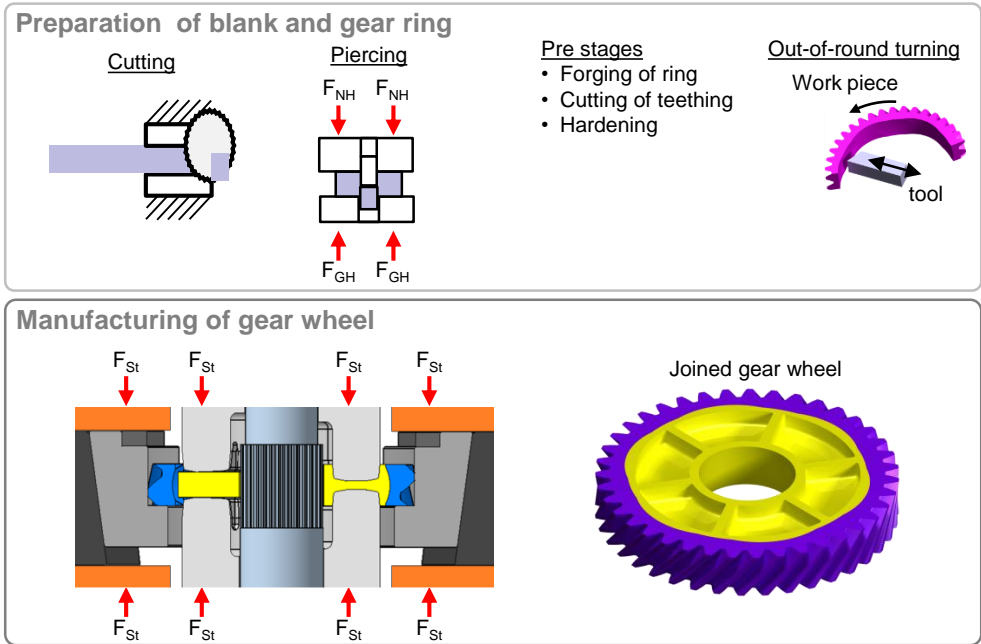

Figure 2.2: Preparation of blank and gear ring; manufacturing of joined gearwheel by lateral extrusion

3   Numerical model setup

This chapter describes the numerical models used to predict the wheel bodies' load potential. To compare the different wheel bodies to each other, they are joined with the gear ring and thereafter the gear ring is loaded with torque. A comparable solid gearwheel is capable of transferring a torque of approximately 400 Nm. Material parameters used for the numerical simulation are shown in table 3.1, as well as the saved weight compared to a solid gearwheel.

3.1   Stapled sheet metal wheel body

3.1.1   Previous investigations

The wheel body is supposed to be at least 25 % lighter than its solid counterpart assuming comparable performance. Using the torque anchor design method by Mattheck [4], a lightweight design to support the load supplied by the gear ring onto the stapled sheet metal wheel body is developed. Figure 3.1 shows the steps of the wheel body's design process. In a first step, every teeth of the gear ring is con-

Table 3.1: Parameters of part, gear ring and simulation parameters

Properties	Unit	Forged	Stapled	Gear ring
Material	[-]	C15	DP-K 700Y980T	18CrNiMo7-6
E-Module	[N/mm²]	210,000	210,000	210,000
Tensile strength	[N/mm²]	400	980	835
Poisson ratio	[-]	0.3	0.3	0.3
Saved weight	[%]	31.5	36.8	

sidered within the design method. The resulting geometry is design one in figure 3.1. Since it is not producible, simplifying the geometry is the second step. Instead of making the number of teeth the main design parameter, a factor of 360 is now serving therefore. In this case, twelve turned out to be a suitable factor, see design two in figure 3.1. It has larger holes than the first one, which allows laser cutting at lower costs. Now that a design is chosen, dimensioning is the next step. Modifying geometry features of the second wheel body (e.g. radii and shape of holes) in several iterations leads to design three. A more homogenized load distribution within the wheel body is recognizable when comparing designs two and three. Design four indicates the design fur further investigations.

after strictly following the design method

after considering producibility and torque

after geometry changes to optimize load distribution

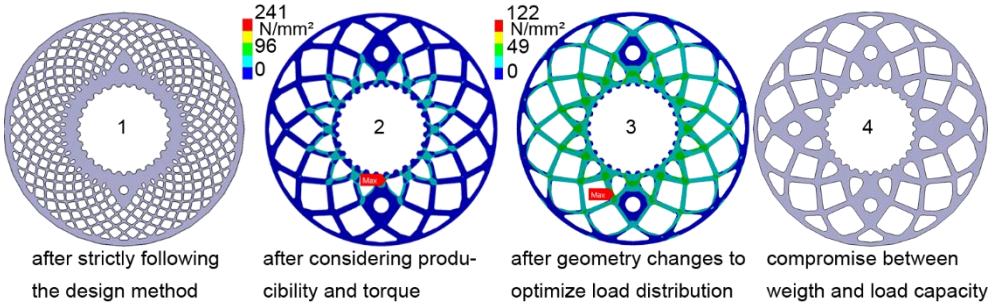compromise between weigth and load capacity

Figure. 3.1: Steps of design optimization of the stapled sheet metal wheel body

3.1.2   Numerical investigations to determine load potential

In Abaqus 6.12-3 an FEM two-stage model is built to investigate the wheel body's load potential. Both stages last one second and use the abaqus standard solver (implicit). To save computation time the gear ring is modelled with three teeth only. Structural meshing of the gear ring is difficult due to the teeth, so it is meshed with tetrahedron elements. The wheel body is meshed using hexahedron elements. (figure 4.1 left) Defining a reference point at the gearwheel's center helps determining the reaction moment later on. Its degrees of freedom are fixed by a boundary condition and the wheel body's gear shaft geometry coupled to it.

Within the first stage the press fit is applied. Interference between gear ring and wheel body is modelled geometrically. Meshing is critical especially in press fit area, as contact behavior tends to become unstable if mesh sizes of contact partners differ largely. Local mesh controls regarding element size ensure the same surface meshes in the contact area on both contact partners. Contact behavior in tangential direction is set to penalty with friction coefficient 0.1. The contact's normal behavior is set to a hard contact. Between the single sheet metal layers, contact behavior is defined using the above settings. Within the simulation model's second stage, a defined displacement in tangential direction is applied as a boundary condition on the gear ring's outer surface. Displacement increases linearly with time until it reaches 0.05 mm by the end of the second stage, which leads to sliding

between gear ring and wheel body. Figure 4.1 (left) depicts the gear wheel's displacement in tangential direction. When the press fit fails, the maximum torque the gear wheel is able to transmit is reached.

3.2   Lateral extruded wheel body

3.2.1   Previous investigations

Previous investigations were related to fundamental process influences and process characteristics. First, the influence of several geometric parameters on the punch force and material are investigated [1]. The investigations are conducted using the materials steel C15 and aluminium Al 1070A. The highest influence is determined to be the wall thickness - the thinner the walls and bridges the higher will be the punch force. Since the lightweight potential is directly dependent on the wall thickness a compromise needs to be figured out. Therefore, the material volume, the punch force as well as the part strength while use need to be targeted at the same time. Regarding the punch force and material flow, the inner gear ring profile, punch segmentation, punch positioning as well as friction show minor influences.

During and after forming high tangential tension stresses will occur at the outer gear ring. In order to prevent failure, a tool is designed to preload the gear ring before the joining process. The preloading is conducted by six segments placed on a slope of the die. The upper tool moves these segments in press direction before the forming process starts. An optimal slope of 8° is figured out to adjust the preloading as precise as possible while preventing self-retention of the segments during the process [2].

Having an epitrochoid profile on the inner side of the gear ring will show high radial displacement differences since the material elasticity mirrors the inner profile under compression. Depending on the profile eccentricity, the gear ring preloading is capable of lowering the radial displacements in total up to 60 %, subsequent grinding will be faster or may be totally prevented [3].

3.2.2   Numerical simulations with different inner gear ring profile designs

In this paper a numerical comparison between two different multi-component gearwheel designs is presented. Regarding the forged gearwheel, two fundamental simulations were conducted – the forming process and a subsequent structural analysis. For the forming process the standard geometric parameters, as depicted in table 3.2, are used. The inner gear ring's epitrochoid profile is between a minimum inner diameter of 73 mm and the outer diameter of 77 mm in order to compare different multi-component gearwheel solutions more accurate by having same dimensions. For this investigation three inner gear ring profiles are used (table 3.2). Both, the blank and the gear ring are regarded elastic-plastic during forming. During the forming process, a constant punch velocity of 100 mm/s is used. After the forming process, each part is separated in order to calculate the geometrical change after spring back. In order to save computing time, the smallest geometry model possible is used considering axial and rotational symmetries. The forming process is simulated using DEFORM 3D^{TM}.

Table 3.2: geometrical parameters of gear ring for forged wheel body

Parameter	dimension
Outer gear ring diameter	94.38 mm
Inner gear ring diameter	73.0 – 77.0 mm
Friction	0.12
Extensions in inner gear ring profile	6
Punch segmentation	6
Wall thickness	3 mm
Eccentricity	V1: 0.7 mm; V2: 2.0 mm; V3: 2.0 mm
Cavity depth	V1: 0.7 mm; V2: 0.7 mm; V3: 2.0 mm

In order to analyse the structural strength, gear ring and wheel body need to be mirrored on the symmetry planes to obtain full bodies. In figure 3.2 the procedure before the structural analysis is depicted.

Model preparation for structural analysis

Forming in DEFORM

Separat elastic springback

Full body geometries for structural analysis

Model postprocessing in Catia
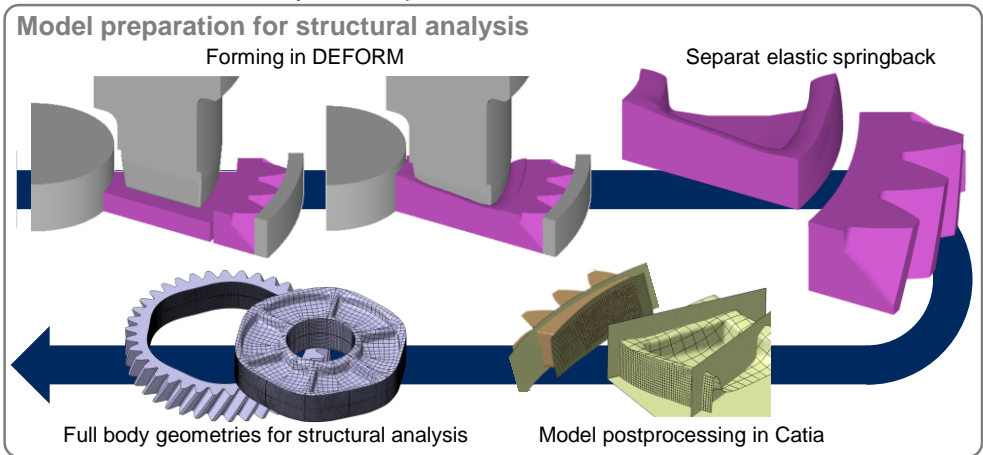
Figure. 3.2: Preparation of formed geometries for structural analysis

3.2.3   Numerical model for structural analysis in Ansys

The structural analysis of the lateral extruded wheel body is processed using AN-SYS. After elastic spring back, the geometries of gear ring and wheel body show interferences at the contacting surfaces. Therefore, an interference adjustment using the elasticity needs to be conducted first. In figure 3.3 the comparison of the contact pressure distribution is depicted after the forming process in DE-FORM 3D^{TM} (left) and after the interference adjustment in ANSYS (right) for an inner gear ring profile having an eccentricity of $e = 2.0$ mm and a cavity of $c = 2.0$ mm. The distribution along the inner surface as well as the absolute contact pressure shows high correlation.

Analysis of geometry transfer

Contact pressure [N/mm²]

500

250

0

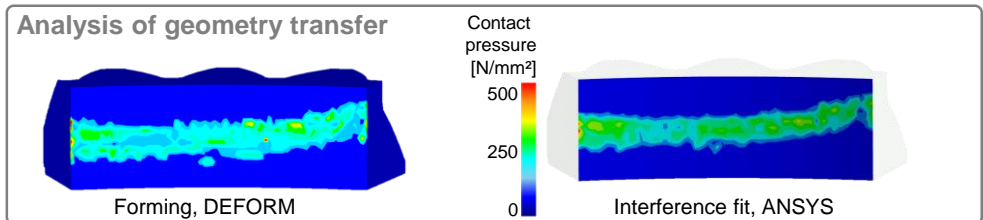Forming, DEFORM

Interference fit, ANSYS

Figure. 3.3:   Display of contact pressure between gear ring and wheel body after forming (DEFORM) and after interference fit (ANSYS)

In order to investigate the effect of torque a fixed bearing is applied on the inside of the gearwheel. Since a torque of 400 Nm is targeted a constant force of 8,858.2 kN is applied at the diameter of 90.31 mm.

4   Results

4.1   Structural analysis of stapled sheet metal wheel body

Figure 4.1 (three pictograms on the right) shows the wheel body's contact pressure and status as well as von Mises stresses right before the press fit fails. As the outer ring of the wheel body is supported at twelve points only, the pressure distribution in the press fit is inhomogeneous. This is due to the changing radial stiffness. Contact status shows that areas with higher contact pressure start to slip later than the ones with lower contact pressure. Therefore, areas in between supporting structures hardly contribute to the press fit. Von Mises stresses are within a range, where the material's possibilities are not yet used completely.
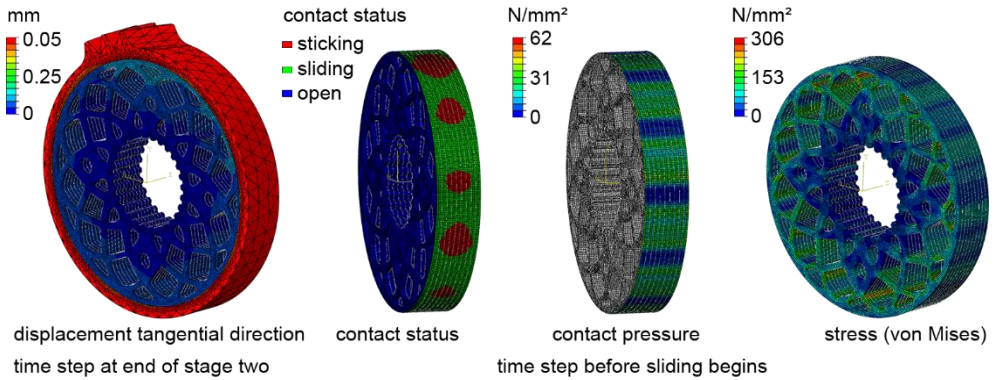

Figure. 4.1: Illustration of the numerical model in Abaqus, contact and stress results

Figure 4.2 shows the numerically determined torque a gearwheel with a stapled sheet metal wheel body can transfer. At the beginning, torque increases linearly with time. Once sliding begins, torque increasing slows down until it reaches a limiting value. This limiting value is 250 Nm. It will be increased by adapting the wheel body's lightweight design, to achieve a homogeneous pressure distribution in the press fit.
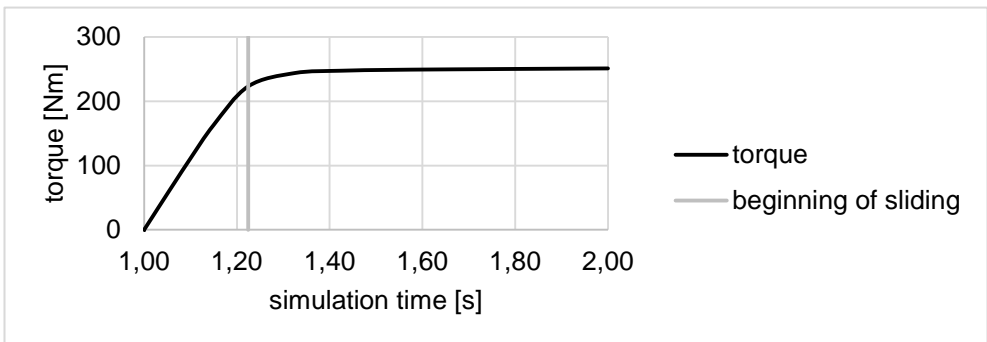

Figure. 4.2: Numerically determined torque the press fit can support

4.2 Structural analysis of lateral extruded (forged) gearwheel body

First, the torque will be examined. In order to proof that the initial torque was transmitted to the shaft the moment reaction and the change of friction needs to be investigated. In order to proof that the torque is transmitted from teething to inner shaft the moment reaction on the inside and the change of friction will be displayed. In figure 4.3 left, the diagram depicts the torque on the teething and the received torque on the shaft. For all three variants, the targeted torque was achieved without any noticeable difference. On the right of figure 4.3 the change of contact status is displayed for version three (eccentricity e = 2.0 mm, cavity of c = 2.0 mm). First, the interference fit will be calculated. During torque application no significant change in contact was detected.
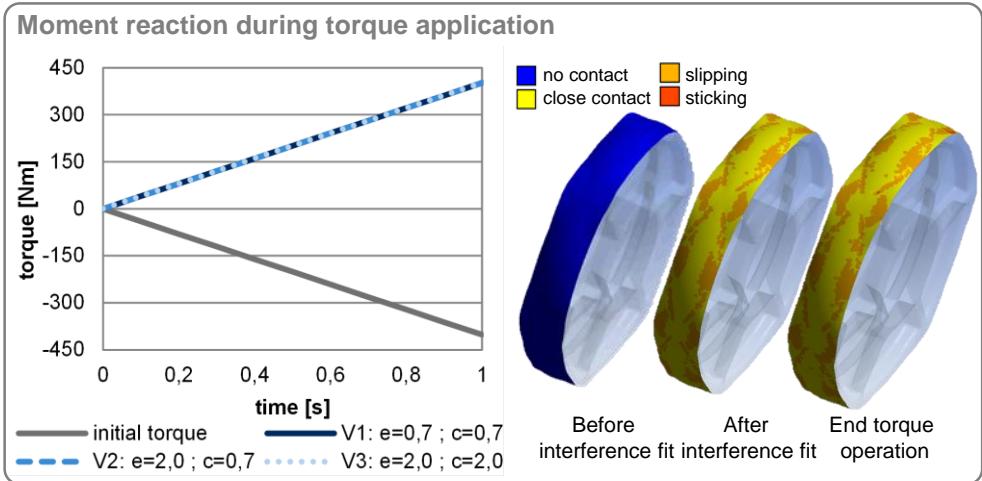

Figure. 4.3: Moment reaction during torque application for three different inner gear ring profiles and corresponding contact status

Figure 4.4 shows the wheel body's displacement, contact pressure and status as well as von Mises stresses at a torque load of 400 Nm. The contact pressure displays a non-uniform distribution along the surface between gear ring and wheel body resulting from the epitrochoid inner profile.
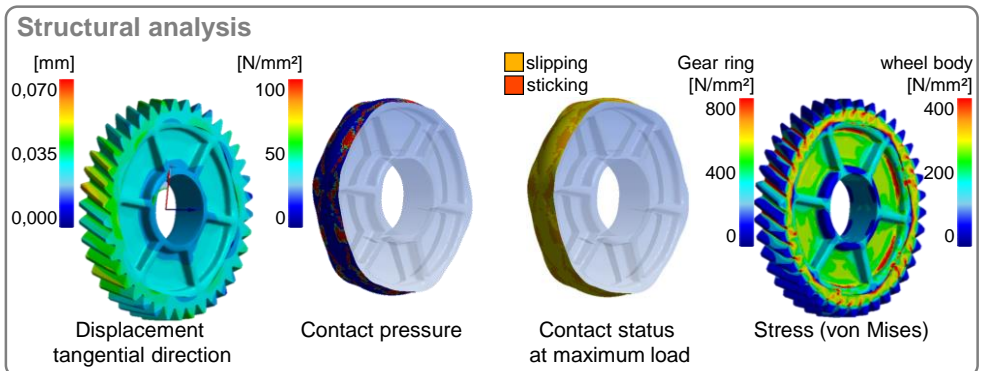

Figure. 4.4: Illustration of the numerical model in Ansys, contact and stress results at 400 Nm torque

The contact status at maximum load displays larger slipping than sticking regions. Sticking regions with high contact pressure occur in areas where the inner gear ring profile has extensions providing an additional form fit. Von Mises stresses are within an acceptable range. The stresses are displayed for the gear ring material 18CrNiMo7-6 and the wheel body material C15 respectively.

5 Conclusion

The two wheel bodies presented in this paper show different torque capacities. While the forged wheel body is supporting the design load completely, the stapled sheet metal alternative fails at 250 Nm due to the press fit. This value might be increased, but simulations with a stapled sheet metal wheel body without a light-weight structure show, that the maximum torque to reach is 325 Nm. So, the forged wheel body is the first choice for high torque. Manufacturing of the stapled sheet metal wheel body will be possible at lower cost though, since there is no need to apply a complex shaped inner surface to the gear ring. Furthermore, blanking tools usually generate more output per time while having a higher lifetime than forging tools. In the end, it will be the end users choice, which wheel body fulfils the requirements best.

6 Acknowledgement

7 References

[1] Meissner, R., Liewald, M., 4.-7. Juli 2016: Numerical investigations of multicomponent lightweigth design for joining gearwheels by lateral extrusion; NUMIFORM 2016, Troyes, Frankreich

[2] Meißner, R., Liewald, M., 2016: Verfahrenskonzept zur umformtechnischen Herstellung von gebauten Zahnrädern im Mehrkomponentenverfahren mittels Quer-Fließpressen, 7. VDI-Fachtagung Welle-Nabe-Verbindungen; Paper reviewed und angenommen

[3] Meißner, R.; Liewald, M.; Weiß, A.: 2016: Numerische Untersuchungen zum Einfluss der Vorspannung auf gefügte Zahnräder; 23. Sächsische Fachtagung Umformtechnik, Dresden

[4] Mattheck, C.; Schäfer, J.: 2010; Denkwerkzeuge nach der Natur; 1. Auflage, Karlsruher Institut für Technologie –Campus Nord